Controllable generation of a spin-triplet supercurrent in a Josephson spin valve

Adrian Iovan, Taras Golod, and Vladimir M. Krasnov*
Department of Physics, Stockholm University, AlbaNova University Center, SE-10691 Stockholm, Sweden
(Received 9 May 2014; revised manuscript received 3 October 2014; published 21 October 2014)

It has been predicted theoretically that an unconventional odd-frequency spin-triplet component of a superconducting order parameter can be induced in multilayered ferromagnetic structures with noncollinear magnetization. In this work, we study experimentally nanoscale devices, in which a ferromagnetic spin valve is embedded into a Josephson junction. We demonstrate two ways of *in situ* analysis of such Josephson spin valves: via magnetoresistance measurements and via *in situ* magnetometry based on flux quantization in the junction. We observe that supercurrent through the device depends on the relative orientation of magnetizations of the two ferromagnetic layers and is enhanced in the noncollinear state of the spin valve. We attribute this phenomenon to controllable generation of the spin-triplet superconducting component in a ferromagnet.

DOI: 10.1103/PhysRevB.90.134514 PACS number(s): 85.75.−d, 74.20.Mn, 74.45.+c, 74.50.+r

I. INTRODUCTION

An interplay of superconductivity (S) and ferromagnetism (F) in hybrid S/F heterostructures leads to a variety of unusual physical phenomena [1–11]. Of particular interest is a possibility of generation of an unconventional odd-frequency spin-triplet component of the superconducting condensate [2,7]. The ferromagnetic exchange energy is usually much larger than the superconducting energy gap. Consequently, a conventional spin-singlet superconducting order parameter decays at a short range ∼1 nm in a spatially uniform, monodomain ferromagnet. Experimental observations of a long-range proximity effect through strong ferromagnets [12,13] and, in particular, through almost fully spin-polarized half-metals [14–16] is consistent with the appearance of the spin-triplet component, which is insensitive to strong magnetic and exchange fields. However, it may also be due to various types of artifacts, and, under certain circumstances, a long-range spin-singlet component can be realized in clean S/F heterostructures [9]. Therefore, unambiguous confirmation for the existence of the spin-triplet superconductivity in S/F heterostructures requires controllable tunability of the phenomenon. This is also a prerequisite for potential applications of S/F heterostructures in spintronics.

The spin-triplet order parameter in S/F heterostructures is generated in the presence of an active spin-mixing interface [5,7] or in the case of a spatially nonuniform distribution of magnetization [2]. The latter can be achieved in spin-valve structures with several F-layers [1,3,6,8–10]. Both the spin-singlet and the spin-triplet components depend on the angle between magnetization of F-layers in such superconducting spin valves. The spin-singlet component is at maximum for the antiparallel (AP) and minimum at the parallel (P) state of the spin valve [9]. The spin-triplet component is maximum at the noncollinear state with 90° misalignment between magnetic moments and zero both in P and AP states [3,8]. Such a behavior has been confirmed by analysis of the inverse proximity effect (i.e., suppression of superconductivity in an S-layer in contact with a ferromagnet) for F/S/F [17,18] and S/F/F [19] structures.

Direct probing of the spin-triplet supercurrent in F-layers requires measurements of perpendicular transport properties through S/F heterostructures [6,8–10]. Even though a supercurrent in such heterostructures has been observed [20–23], conclusive evidence for the spin-triplet nature of the supercurrent is still missing due to a difficulty with separation of singlet and triplet components and due to the general complexity of such a device with several degrees of freedom, the influence of stray fields, and Josephson vortices. Interpretation of the data becomes particularly difficult in the case of polydomain switching of the spin valve [4,21]. Consequently, for unambiguous interpretation of the data, it is necessary to study small monodomain structures and to establish accurate *in situ* characterization techniques.

Here we study nanoscale Josephson spin-valve devices, in which a spin valve is implemented as a barrier in a Josephson junction. We describe two methods for *in situ* characterization of devices using (i) perpendicular magnetoresistance and (ii) *in situ* magnetometry based on flux quantization in a Josephson junction. In this way, we unambiguously prove that the critical current is enhanced in the noncollinear state of the spin valve, which is consistent with a controllable generation of the spin-triplet order parameter.

II. EXPERIMENT

We study two types of Josephson spin valves, consisting of two dissimilar CuNi ferromagnetic layers $F_{1,2}$ separated by a spacer layer of either a normal metal (N) Cu or a thin superconductor (S′) Nb. A scanning electron microscope (SEM) image and a sketch of the structures are shown in Figs. 1(a) and 1(b). The two ferromagnetic layers are made dissimilar in order to achieve different coercive fields, required for controllable switching of magnetization in the spin valve. This is also necessary for generation of the spin-triplet component of the supercurrent. In the symmetric SFFS Josephson spin valve, the spin-triplet component cancels out, but in the dissimilar SF_1F_2S junction it remains finite [8].

The SF_1NF_2S ($Nb/Cu_{0.5}Ni_{0.5}/Cu/Cu_{0.4}Ni_{0.6}/Nb$ 200/10/20/10/200 nm) and $SF_1S'F_2S$ ($Nb/Cu_{0.5}Ni_{0.5}/Nb/Cu_{0.4}Ni_{0.6}/Nb$ 200/10/10/10/200 nm) multilayers were deposited by dc-magnetron sputtering in a single deposition cycle without breaking vacuum. The

*Vladimir.Krasnov@fysik.su.se

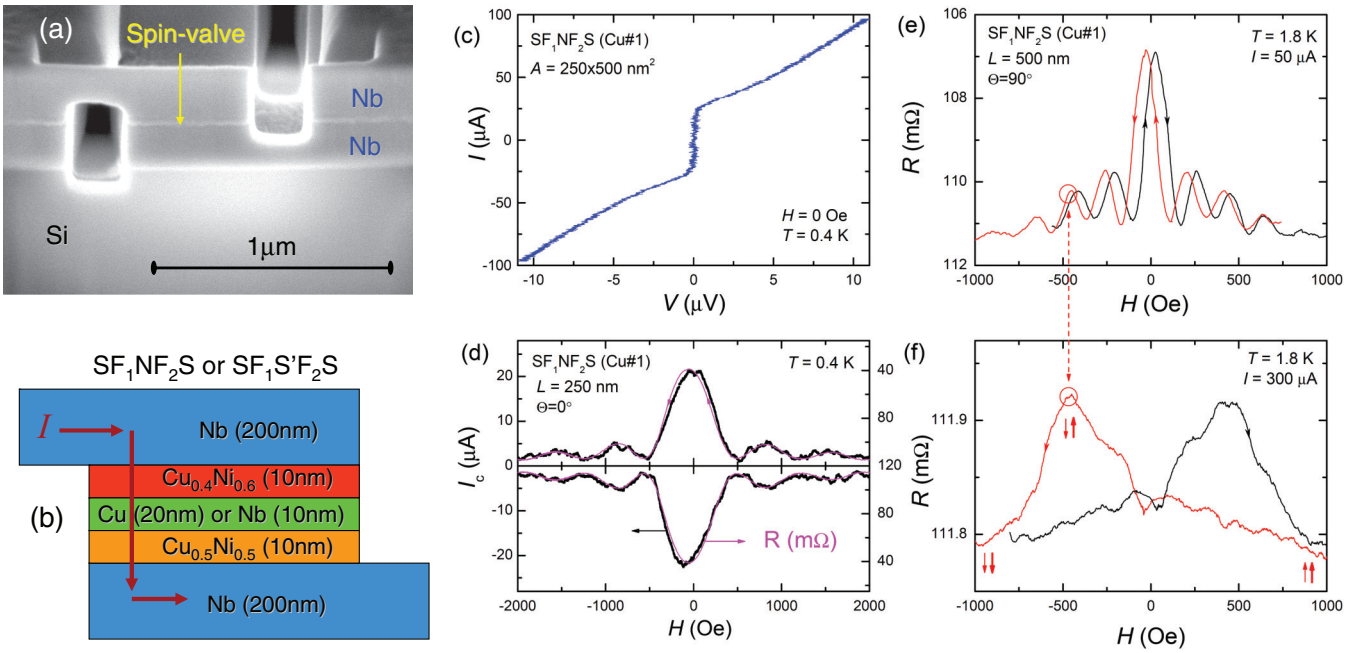

FIG. 1. (Color online) Characterization of Josephson spin valves. (a) SEM image of a device. (b) A sketch of studied structures. (c) Current-voltage characteristics of an SF_1NF_2S junction (Cu#1) at zero field. (d) Fraunhofer modulation of the Josephson current (black symbols) and a low-bias resistance (magenta lines) at $T = 0.4$ K. (e) Low- and (f) high-bias resistance of the same junction vs magnetic field for upward (black) and downward (red lines) field sweeps at $T = 1.8$ K. It is seen that we can study both the Josephson current and the spin-valve magnetoresistance by changing the bias level. A hysteretic behavior of the spin valve is clearly seen in both plots. Circles indicate the AP state for the downward field sweep.

$Cu_{1-x}Ni_x$ films were deposited by cosputtering from Cu and Ni targets. Nanoscale junctions with sizes down to 100 nm were patterned by photolithography, reactive ion etching, and three-dimensional nanosculpturing using a focused ion beam, as described in Ref. [24]. Small dimensions were necessary both for monodomain switching of spin valves (see an additional discussion of domain sizes in SFS structures in Appendix A) and for enhancement of junction resistances to comfortably measurable values. Measurements were done either in a He-3 cryostat or in a He-4 gas flow cryostat. We define the angle $\Theta = 0^\circ$ and 90° when the magnetic field is applied along and perpendicular to the long side of the junction, respectively. In all cases, the magnetic field is parallel to the junction plane. In total, more than ten devices were studied. The data below are representative for all of them.

III. RESULTS AND DISCUSSION

Figure 1(c) shows current-voltage (I-V) characteristics of an SF_1NF_2S junction (Cu#1 $\sim 250 \times 500$ nm^2) at $H = 0$ and $T = 0.4$ K. A critical current $I_c \simeq 25$ μA is clearly seen. It corresponds to a critical current density $J_c \simeq 2 \times 10^4$ A/cm^2. Black symbols in Fig. 1(d) represent the magnetic-field dependence of the critical current at $\Theta = 0^\circ$. The field is swept from positive to negative values. A clear Fraunhofer-type $I_c(H)$ modulation proves the Josephson nature of the supercurrent through the spin valve. It indicates good homogeneity of I_c and a monodomain structure of F-layers [21] [see an additional discussion of the detrimental effect of domains on $I_c(H)$ modulation in Appendix C]. The supercurrent rapidly decreases with increasing T and becomes difficult to measure at $T > 2$ K. To improve the resolution, we performed lock-in measurements of resistance with a small bias of the order of I_c. The corresponding $R(H)$ modulation is shown by magenta lines in Fig. 1(d) (right axis). It is seen that $I_c(H)$ is equivalent to the $R(H)$ data after appropriate rescaling (reverse scale, large R corresponds to small I_c). Since the noise level is much smaller for lock-in measurements, in what follows we will use low-bias resistance for characterization of I_c.

Figure 1(e) shows the $R(H)$ modulation for the same SF_1NF_2S junction at $\Theta = 90^\circ$ and $T = 1.8$ K. Measurements were performed with a low ac-current amplitude $I = 50$ μA. Here we can clearly see a hysteresis between the upward (black) and downward (red) field sweeps, which is due to remanence magnetization of the spin valve. At higher fields (not shown), Abrikosov vortices may be trapped in S-electrodes. As discussed in Ref. [24], vortex-induced hysteresis is opposite to remanence magnetization and, therefore, can be clearly distinguished. All the data presented here are for the vortex-free case. The absence of vortices indicates that the magnetization from F-layers does not puncture S-layers, but is forced to lie in-plane despite the possible perpendicular anisotropy of magnetization in CuNi thin films [25] (see an additional discussion of magnetic anisotropy in Appendix B).

Figure 1(f) shows the high-bias resistance, measured for the same configuration as in Fig. 1(e) but with a large ac current $I = 300$ μA $\gg I_c$. In this case, we measure predominantly the normal resistance R_n at the Ohmic part of the I-V. It is seen that $R_n(H)$ represents a spin-valve magnetoresistance with minima and maxima at P and AP orientations of magnetizations in the two ferromagnetic layers, respectively [20,26]. From Figs. 1(e)

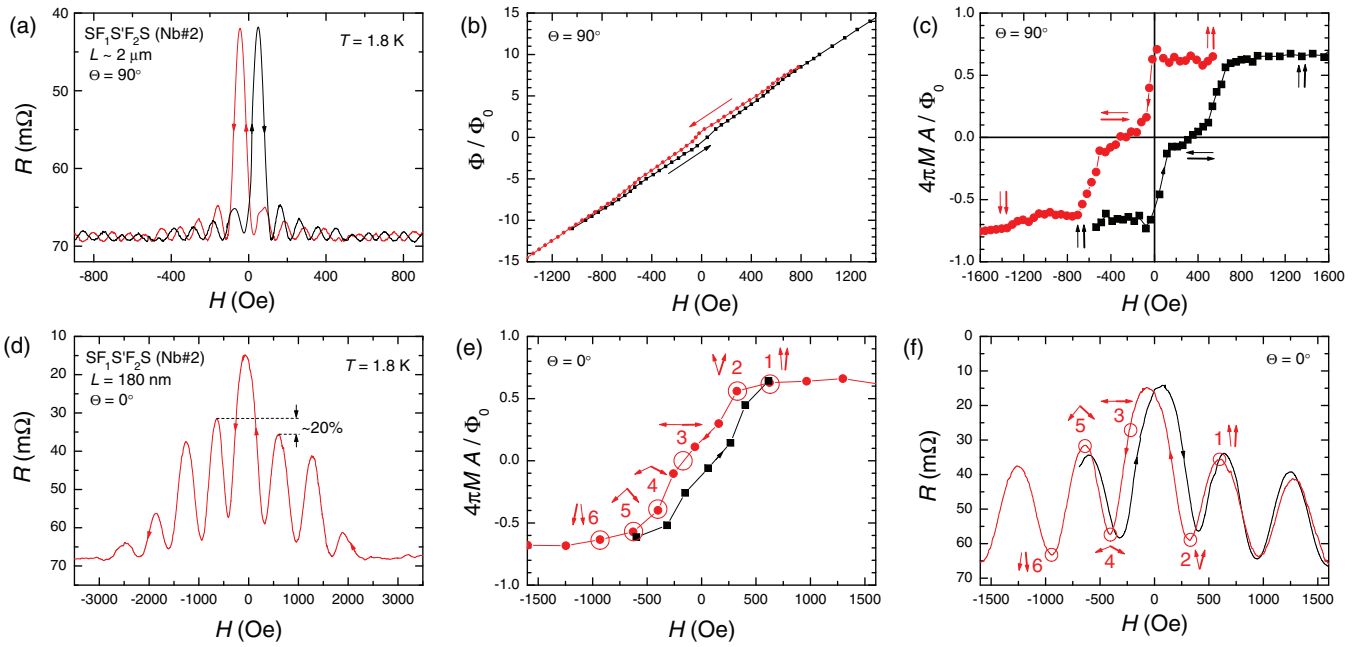

FIG. 2. (Color online) Properties of $SF_1S'F_2S$ junction. (a) Fraunhofer modulation of $R(H)$ at $\Theta = 90^\circ$ for upward (black) and downward (red line) field sweeps. (b) Magnetic-field dependences of the flux in the junction. Each point represents integer or half-integer Φ_0, corresponding to maxima or minima in $R(H)$ from panel (a). (c) Magnetization curves at $\Theta = 90^\circ$, obtained from the data in panel (b). The intermediate step with $M \sim 0$ corresponds to the AP state of the spin valve. (d) Fraunhofer modulation of $R(H)$ at $\Theta = 0^\circ$ for the downward field sweep. (e) The magnetization curves at $\Theta = 0^\circ$. Arrows indicate orientations of magnetization in the spin valve at points 1–6 for the downward field sweep. (f) Central part of the Fraunhofer modulation of $R(H)$ at $\Theta = 0^\circ$ for upward (black) and downward (red line) field sweeps. Note the asymmetry of the Josephson current at points 1 and 5, corresponding to the same $|\Phi/\Phi_0| = 1.5$. The asymmetry is attributed to generation of an additional spin-triplet component of the supercurrent in the noncollinear state of the spin valve.

and 1(f) it is seen that we can measure both the critical current and the magnetoresistance by changing the bias current level. Circles in Figs. 1(e) and 1(f) indicate the AP state of the spin valve for the downward field sweep. Thus we have successfully realized the Josephson spin valve, exhibiting both the spin-valve effect and the Josephson supercurrent.

Figure 2 represents data for an $SF_1S'F_2S$ junction (Nb#2 $\sim$180 nm $\times$ 2 μm) at $T = 1.8$ K. Figures 2(a) and 2(d) represent $I_c(H)$ [low bias $R(H)$] modulations for magnetic-field orientations perpendicular to the long ($\Theta = 90^\circ$(and the short ($\Theta = 0^\circ$) sides of the junction, respectively. Minima and maxima of $I_c(H)$ [maxima and minima of $R(H)$] correspond to integer and half-integer flux quanta Φ_0 within the junction. In $SF_1S'F_2S$ junctions, the spin-valve magnetoresistance is hardly detectable [unlike SF_1NF_2S junctions, Fig. 1(f)], probably due to a much shorter scattering time in Nb than in Cu. Therefore, we employ a different method for determination of the spin-valve configuration in $SF_1S'F_2S$ junctions, following Ref. [27], in which it was demonstrated that flux quantization in a Josephson junction can be used for *in situ* analysis of magnetization.

In Fig. 2(b) we plot the flux through the junction as a function of applied magnetic field for the data from Fig. 2(a). Here every point corresponds to a maximum or a minimum of $R(H)$. Apparently it represents the $B(H) = H + 4\pi M(H)$ curve integrated over the junction cross-section area A. At high fields, when both F-layers are saturated in the P-state, the $B(H)$ becomes linear. Subtracting this linear dependence, we can obtain the magnetization curve $M(H)$. Thus our junctions operate as *in situ* magnetometers (absolute fluxometers) for our nanoscale spin valves.

Figures 2(c) and 2(e) show the thus obtained magnetization curves for the two field orientations. From Fig. 2(c) it is seen that upon sweeping of the magnetic field, the magnetization of the spin valve switches via two steps. This is a standard behavior of a monodomain spin valve [26] in a so-called scissors state. In this case, the magnetizations of the two layers are rotating in opposite directions (see an additional discussion about the spin-valve switching and the corresponding numerical simulations in Appendix D). At $200 < H < 500$ Oe there is a plateau with $M \sim 0$. It represents the AP state of the spin valve, as indicated in the figure. In Fig. 2(e) the behavior is similar, even though the plateau is less defined.

Red arrows in Fig. 2(e) indicate the relative orientations of magnetization in the two F layers for downward sweeping of the field. At a large positive field, point 1, the spin valve is close to the up-up parallel state. At point 2, moments are slightly rotated away from the P state. At point 3, the magnetization becomes close to zero, which implies that the spin valve has switched into the AP state. At larger negative fields, points 4 and 5, the moments continue to rotate downward, and at point 6 the spin valve is close to the down-down parallel state. Thus we can trace the state of the spin valve from the *in situ* magnetization measurement. This completes the characterization of the spin valve in our junctions, and we can now proceed to our main topic, namely a discussion of controllable realization of the spin-triplet component of the supercurrent.

In Fig. 2(f) we replot the central part of the $I_c(H)$ [inverted $R(H)$] modulation at $\Theta = 0^\circ$, in which we marked the positions and magnetization orientations for points 1–6 from Fig. 2(e). It is seen that for the downward field sweep (red line), the critical current at point 1, which correspond to $\Phi \simeq 1.5\Phi_0$, is smaller than at point 5, which correspond to $\Phi \simeq -1.5\Phi_0$. The asymmetry is also seen for other maxima of I_c at half-integer Φ_0 in Fig. 2(d). For the downward field sweep, all the maxima of I_c at negative fields are larger than the corresponding maxima at positive fields with the same absolute value of Φ/Φ_0. As a consequence of this asymmetry, there are four lobes at the negative side and only three lobes at a positive side of the $I_c(H)$ modulation in Fig. 2(d). The asymmetry is reversed for the upward field sweep, shown by the black line in Fig. 2(f). For the SF_1NF_2S junction (Cu#1), the same type of asymmetry is seen from Fig. 1(e). The field sweep direction-dependent asymmetry of $I_c(H)$ was observed in all studied Josephson spin-valve structures, and it is our central observation.

The observed left-right asymmetry of $I_c(H)$ is different from the centrosymmetric $I_c(H)$ asymmetry caused by inhomogeneity of junction parameters [11,28], which does not depend on the direction of the field sweep. We emphasize that such asymmetry was not present in our SFS junctions made with the same technique and with the same dimensions, but containing only one F-layer [see e.g., Fig. 4(b) from Ref. [24]]. Consequently, the asymmetry is not the property of the individual F-layers, but it is related to the history-dependent orientation of the spin valve (see additional supporting arguments in Appendix E).

It is important to note that points 1 and 5 in Fig. 2(f) correspond to exactly the same absolute value of the flux $|\Phi/\Phi_0| \simeq 1.5$. Consequently, the asymmetry is entirely due to a different orientation of magnetization in the spin valve. As shown in Figs. 2(e) and 2(f), at point 1 the spin valve is close to the P-state, while at point 5 it is in the noncollinear angle state. From the theoretical analysis it follows that the spin-triplet component of supercurrent has a maximum in the noncollinear state of the SF_1F_2S junction with dissimilar ferromagnets [8]. Therefore, the observed direction-dependent asymmetry of the supercurrent is consistent with a controllable generation of the spin-triplet component in our Josephson spin valves. The magnitude of asymmetry indicates that the amplitude of generated spin-triplet supercurrent is rather small, in the range of 10–20 % of the main spin-singlet part of the supercurrent. This is expected because in SF_1F_2S structures, the spin-triplet supercurrent is only due to the dissimilarity of the $F_{1,2}$ layers [8], which is not large in our case. On the other hand, the dominant singlet component is beneficial for our analysis. Singlet and triplet components of the Josephson current are harmonic and double-harmonic, correspondingly, with respect to the Josephson phase difference [8]. Therefore, the dominant spin-singlet component enables a regular, periodic in Φ_0, Fraunhofer $I_c(\Phi)$ modulation and facilitates accurate characterization of our spin valves via *in situ* fluxometry, as shown in Fig. 2(c).

To conclude, we have successfully fabricated SF_1NF_2S and $SF_1S'F_2S$ Josephson junctions with embedded nanoscale spin-valve structures. We demonstrated that such Josephson spin valves exhibit both the supercurrent and the spin-valve magnetoresistance, both of which depend on the relative orientation of magnetization of the two ferromagnetic layers. Flux quantization in such structures was employed for *in situ* measurement of magnetization of the spin valve. Our main result is the observation of an asymmetry of the critical current with respect to the direction of sweeping of the magnetic field, which depends solely on the orientation of the spin valve. In the noncollinear state of the spin valve, we observed an increase of the Josephson supercurrent, which we attributed to controllable generation of the spin-triplet component of the order parameter.

Note added. Recently, we became aware of another publication on a similar subject [29].

ACKNOWLEDGMENTS

We are grateful to A. Rydh for assistance with the experiment, and Ya. Fominov for a valuable discussion. Technical support from the Core Facility in Nanotechnology at Stockholm University is gratefully acknowledged.

APPENDIX A: DOMAIN SIZE IN SFS STRUCTURES

Controllable generation of a spin-triplet order parameter requires a monodomain state of a spin valve. The critical size at which a small ferromagnetic particle switches into the monodomain state is not necessarily correlated with the domain size in a wide film because demagnetization effects in the two cases are different. The critical size can be both smaller and larger than the domain size in a wide film [30]. Nevertheless, it is instructive to analyze the domain sizes in a films. For thick films, the domain size D is decreasing proportionally to the square root of the films thickness $D \propto \sqrt{d_F}$. But for very thin films, $d_F \ll D$, the tendency is reversed and D starts to rapidly increase with decreasing d_F. As shown in Ref. [31] in the thin-film limit,

$$D \simeq d_F \exp\left(\frac{\pi D_0}{2d_F}\right), \tag{A1}$$

where D_0 is the smallest domain size at the transition from the thick- to the thin-film limits.

In SFS heterostructures, S-layers screen the stray magnetic fields from the F-layer. This changes the demagnetization energy and affects the domain size [32,33]. In the thick-film limit, the domain size is reduced by a maximum $1/\sqrt{2}$ factor. But in the thin-film limit, the increase of D with decreasing d_F becomes faster than for a single F-film, Eq. (A1). Furthermore, below a certain critical thickness $d_c \sim D_0$, a phase transition into a uniform (monodomain) state should occur [32,33]. Such an abrupt transition from a polydomain to a monodomain state does not occur in a single F-film, but only in SF or SFS structures. Roughly speaking, it is expected that the F-layer within the SFS structure is monodomain as soon as the thickness of the F-layer is (significantly) smaller than the domain size in the individual F-layer.

Veshchunov *et al.* performed direct visualization of the domain structure in CuNi thin films using a decoration technique [25]. They observed a mazelike domain structure with the domain width $D \sim 100$ nm for the $Cu_{0.47}Ni_{0.53}$ film with thickness $d_F \simeq 20$ nm. From Eq. (A1) it follows

that films with $d_F = 10$ nm, used in our devices, would have the equilibrium domain size of $D \sim 250$ nm, which is in the range of the sizes of our devices. Furthermore, in Ref. [34] it was reported that the domain size in 20-nm-thick $Cu_{0.47}Ni_{0.53}$ films increases when the film is deposited on a superconductor. It confirms that $d_F = 20$ nm films are already in the thin-film limit for magnetic domains. According to theoretical calculations [32], our twice thinner $d_F = 10$ nm films, sandwiched between thick superconducting electrodes, should be in the monodomain state.

APPENDIX B: MAGNETIC ANISOTROPY

Crystalline and shape anisotropies determine the orientation of easy and hard axes of magnetization. A relative orientation of applied field with respect to those axes plays a significant role in the dynamics of magnetic nanostructures. Magnetization loops along the easy axis are characterized by an abrupt switching and a large hysteresis. On the contrary, for a field along the hard axis, the magnetization is changing gradually with a small or no hysteresis.

The shape anisotropy is determined by demagnetization effects. For a single particle, easy and hard axes coincide with long and short sides of the particle, respectively [35,36]. Inspection of $M(H)$ curves from Figs. 2(c) and 2(e) reveals an unusual shape anisotropy of our junctions: it is more easy-axis-like for a field applied along the shortest side of the structure. There can be several reasons for that. (i) First, in the presence of superconducting capping, the moment is forced to flip in-plane. The resulting shape anisotropy of the SFS structure is strongly affected by thick superconducting electrodes because their demagnetization factors are largely different from that for a thin F-film. (ii) In the AP state of a spin valve, demagnetizing fields become insignificant, which should affect the shape anisotropy. That is, the shape anisotropy in the P- and the AP-states may be different. (iii) We do not exclude a possible influence of stray fields from bulk electrodes in the vicinity of a spin valve; see Fig. 1(a). (iv) The unusual shape anisotropy can be caused by a nontrivial intrinsic (crystalline and structure-related) anisotropy of CuNi films.

The behavior of intrinsic anisotropy is rather complicated. It depends on the morphology and the columnar structure of the films, which in turn depends on the fabrication procedure. The easy axis often flips from the in-plane to the out-of-plane orientation upon changing the film thickness [30]. For binary ferromagnetic alloys, the anisotropy may depend on the composition. In Ref. [38] it was shown that the anisotropy of $Pt_{1-x}Ni_x$ thin films changed from out-of-plane to canted and then to in-plane with increasing Ni concentration above critical value for the appearance of the ferromagnetism, $x_c \simeq 0.4$. Similar behavior is likely to occur in CuNi thin films. Indeed, an out-of-plane anisotropy was reported for $Cu_{0.47}Ni_{0.53}$ thin films [25]. However, $Cu_{0.43}Ni_{0.57}$ films with slightly larger Ni concentration, studied in Ref. [39], exhibited a large hysteresis in the in-plane field, indicating an in-plane anisotropy (orientation of the easy axis). Pure Ni films have an in-plane anisotropy at any thickness [40]. The out-of-plane intrinsic anisotropy would make both in-plane axes hard.

To understand the magnetic anisotropy of our F layers, we have studied the Hall effect in CuNi films with the same compositions and thickness as in our spin valves. We found out that such films have a very weak out-of-plane anisotropy. However, if the films are initially magnetized in-plane, the moment remains in-plane even after removing the field. Simultaneously, we observed a long superparamagnetic tail at temperatures above the Curie temperature, indicating the presence of small Ni clusters 3–4 nm in size. At intermediate temperatures, the films exhibit cluster/spin glass behavior [37,38]. At low temperatures $T < 20$ and $\sim$100 K for $Cu_{0.5}Ni_{0.5}$ and $Cu_{0.4}Ni_{0.6}$, respectively, both films behave like ferromagnets with the size of hysteresis similar to that in Figs. 1(f), 2(c), and 2(e). However, the coercive field is almost independent on the field orientation. Most likely small clusters are responsible for the lack of the shape anisotropy in such films. A detailed analysis of the magnetic properties of CuNi thin films will be published later [41].

All the mentioned affects are likely to play a role in the observed unusual shape anisotropy in our structures. We want to emphasize, however, that irrespective of the origin of the unusual shape anisotropy, we do not need to guess about the relative orientation of the two ferromagnetic layers because the *in situ* magnetization measurements, shown in Fig. 2, provide explicit information about the state of the spin valve. This is an important advantage of our study.

APPENDIX C: EFFECT OF DOMAINS ON THE $I_c(H)$ MODULATION

The $I_c(H)$ modulation curves shown in the paper exhibit a regular Fraunhofer-type modulation. The behavior of our Josephson spin valves is fully consistent with the monodomain (scissors-type) state of the spin valves, as demonstrated in the following appendix. The appearance of domains strongly distorts the $I_c(H)$ modulation because it disrupts the spatial uniformity of the magnetic field inside the junction. This has been demonstrated in previous works on larger SFS junctions [27,42].

Figure 3 demonstrates the strongly detrimental effect of (artificially introduced) domains on the $I_c(H)$ patterns of our Josephson spin valve. To destroy the spatial uniformity of the F-layers, we utilized strong attractive interaction between domain walls in F-layers and Abrikosov vortices in S-layers [43]. Therefore, the introduction of vortices stabilizes the polydomain state. To introduce vortices, we applied a magnetic field perpendicular to the film. Figure 3 represents measurements upon a sweep from a large positive to a negative out-of-plain field. Curves with different colors represent two consecutive sweeps under identical conditions. Initially a large amount of vortices is present in S-films, and the magnetization in F-layers is saturated out-of-plane. With a reduction of the field, vortices start to leave S-layers, and F-layers start to remagnetize. However, due to a strong pinning between vortices and domain walls, remagnetization in this case occurs via the appearance of domains and propagation of domain walls along F-layers. Each time the domain wall crosses the edge, a large bundle of vortices pinned at the domain wall leaves the structure. This causes abrupt and irregular (not

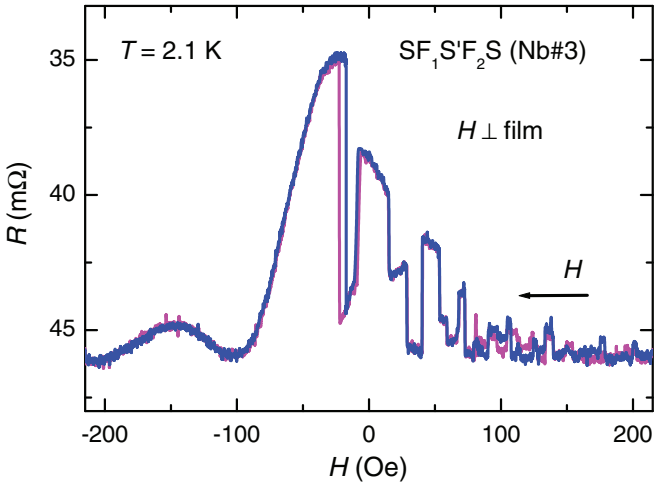

FIG. 3. (Color online) Measured low-bias resistance vs out-of-plain magnetic field for a junction Nb#3. Curves with different colors represent two identical measurements during sweeps from positive to negative field. At large positive field, Abrikosov vortices enter S-layers. Pinning between vortices and domain walls leads to the appearance of the polydomain state with irregular $I_c(H)$. Upon exit of vortices at a small negative field, F-layers return in the monodomain state and a regular $I_c(H)$ modulation is restored.

reproducible) jumps in $I_c(H)$ until all vortices leave the sample at a small positive field and the F-layers return into the uniform monodomain state. Only then is a regular Fraunhofer-like modulation of $I_c(H)$ restored.

APPENDIX D: NUMERICAL MODELING OF SPIN-VALVE CHARACTERISTICS

The effects discussed in the paper depend essentially on the details of switching of the spin valve. To clarify how to distinguish different types of switching, we performed extended micromagnetic calculations for various parameters of spin valves (exchange coupling, magnetization, anisotropy, shape, size) [44]. The output is demonstrated in Fig. 4. There are two basic types of spin-valve switching, i.e., monodomain (coherent rotation or scissors state) and polydomain, and their characteristics are represented in panels (a)–(c) and (d)–(f), respectively. In calculations, we adopted parameters typical for our structures, including different intrinsic anisotropies of the two layers, as discussed above. To obtain the polydomain state, we increased the size of the structure ten times, keeping the same aspect ratio. The effect of superconducting electrodes is not considered.

In the scissors case, the magnetizations of the two layers are rotating in opposite directions upon reduction of the magnetic field without splitting into domains, as seen from Fig. 4(c). Figure 4(b) demonstrates that the rotation leads to the appearance of an orthogonal component to the field components of magnetization M_{y1} and M_{y2} of opposite signs. They reach maxima in the AP state (point B) with values close

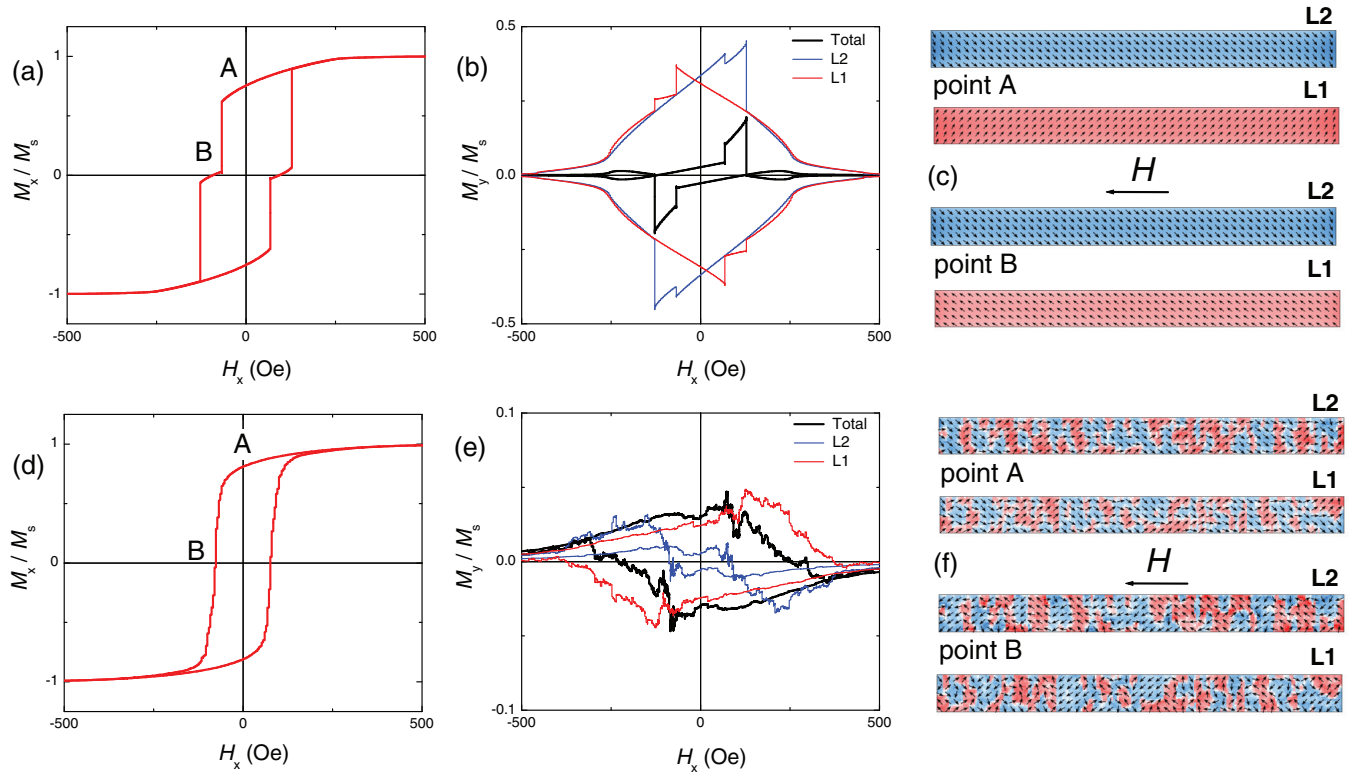

FIG. 4. (Color online) Micromagnetic simulations of spin-valve characteristics with parameters typical for our junctions (a)–(c) in the monodomain scissors case and (d)–(f) in the polydomain case (for ten times larger sizes). Note that an AP step in the magnetization curve $M_x(H_x)$ appears only in the monodomain case. Panels (c) and (f) represent top views of magnetization distribution at points A and B, marked in panels (a) and (d).

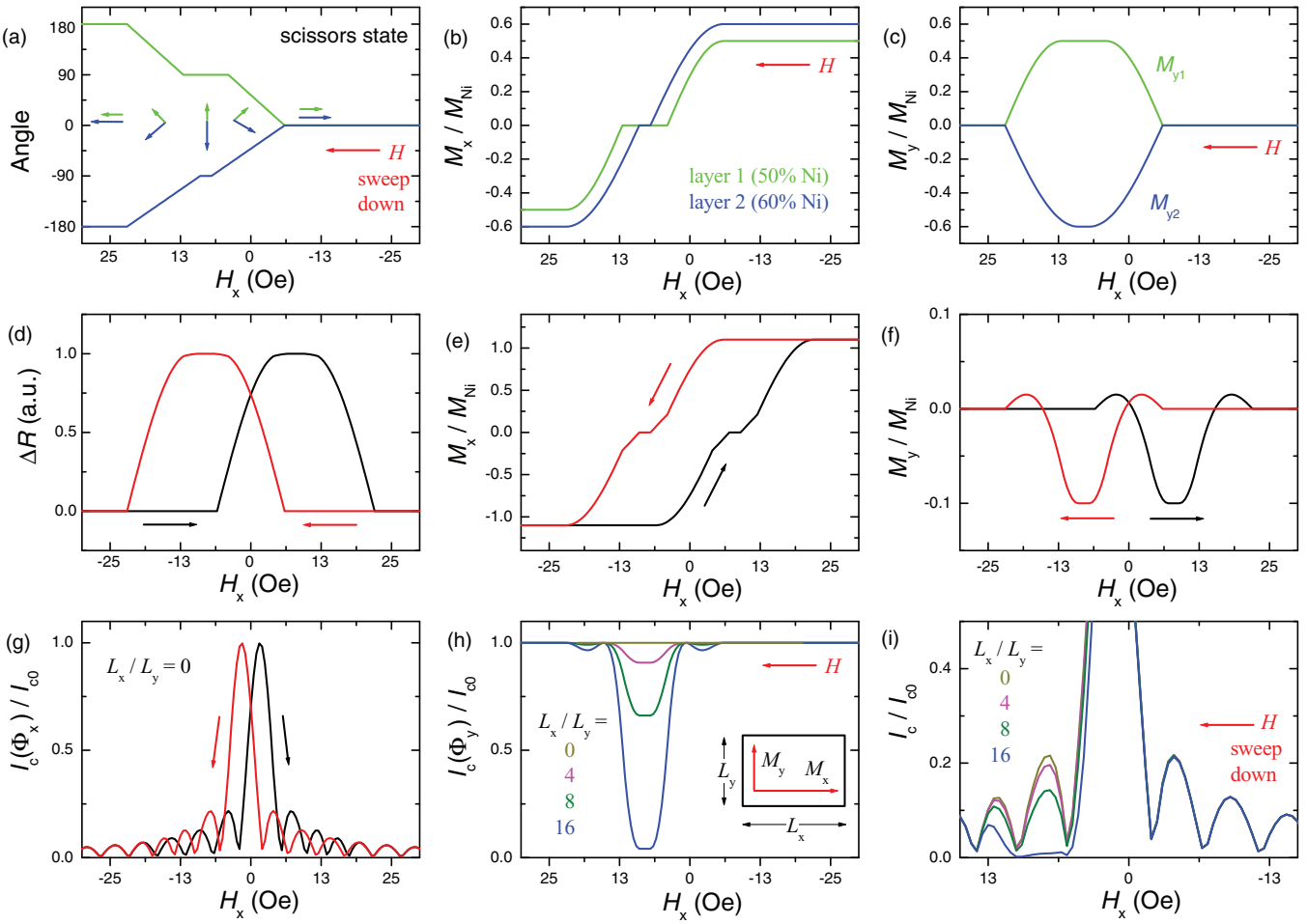

FIG. 5. (Color online) Analysis of the influence of the orthogonal to the field magnetization on the $I_c(H)$ modulation for a simplified scissors state model of a Josephson spin valve. (a) Angles of magnetization of the two layers. (b) and (c) Magnetizations of layers along (a) and orthogonal (b) to the field. (d) Spin-valve magnetoresistance. (e) and (f) Total magnetization along and orthogonal to the field. Note a close resemblance of both magnetoresistance (d) and magnetization (e) curves with experimental data in Figs. 1(f) and 2(c). The maximum of the orthogonal M_y component corresponds to the AP state of the spin valve (f). The influence of the M_y on $I_c(H_x)$ depends on the aspect ratio of the junction L_x/L_y. Panel (g) represents the case without distortion by M_y. Panel (h) shows solely the influence of the M_y component for different aspect ratios. Panel (i) shows the $I_c(H_x)$ modulation, taking into account the M_y component for the downward field sweep. It is seen that M_y tends to suppress I_c close to the AP state, which is *opposite* to our experimental observation.

to the corresponding saturation magnetizations. The energetic stability of the AP state leads to the appearance of a pronounced step with $M_x \sim 0$ in the magnetization curve $M_x(H_x)$, as seen from Fig. 4(a).

In the polydomain case, domains are changing in size and orientation upon remagnetization, as shown in Fig. 4(f). Since domains compensate for each other, the polydomain switching does not produce a significant orthogonal component of the moment M_y, as seen from Fig. 4(b). There is no true AP state, and the magnetization curve $M_x(H_x)$ does not have an intermediate AP step, as seen from Fig. 4(a). This is contrary to our experimental observations. The presence of a well-defined middle step in $M(H)$ serves as a good indication of the monodomain switching of the spin valve. Consequently, switching of our nanoscale spin valves is not consistent with the polydomain scenario.

The appearance of the orthogonal M_y magnetization in the scissors state may affect the measured critical current because it will induce an additional flux through the junction [45]. To understand whether such a trivial effect could be confused with generation of the spin-triplet component of the order parameter, in Fig. 5 we present corresponding numerical calculations for a simplified model of scissors switching. Figure 5(a) shows the angles of magnetization of the two layers upon remagnetization from the positive P (0°) to the negative P (±180°) states. Figures 5(b) and 5(c) represent the corresponding magnetization curves along and perpendicular to the field, respectively. Magnetization is normalized by the saturation magnetization of Ni, M_{Ni}. We assumed that saturation magnetization is proportional to Ni concentration in our films, i.e., 0.5 and 0.6 M_{Ni}, correspondingly.

Figures 5(d) and 5(e) show the spin-valve magnetoresistance and the total magnetization along the field. There is a well-defined intermediate step in $M_x(H_x)$, which corresponds to the AP state of the spin valve with $M_x = 0$. Those curves are qualitatively similar to experimental data in Figs. 1(f), 2(c), and 2(e). Thus, both *in situ* magnetoresistance and magnetization measurements are consistent with

monodomain scissor-type switching of our spin valves. This is important because it facilitates a well-defined noncollinear state, required for generation of the spin-triplet component of the order parameter. Figure 5(f) shows the total magnetization orthogonal to the field. In the AP state, it reaches the maximum value $|M_y = M_1 - M_2| = 0.1M_{\rm Ni}$, which is much less that the saturation value $M_1 + M_2 = 1.1M_{\rm Ni}$.

The influence of the orthogonal component M_y on $I_c(H_x)$ depends on the size of the junction L_x because the total flux $\Phi_y = 4\pi M_y L_x \Lambda_M$, where Λ_M is the effective magnetic thickness of the structure. Figure 5(g) represents simulation of $I_c(\Phi_x)$ for $L_x = 0$, when there is no influence of the M_y component. We adjusted the product $M_x L_y \Lambda_M$, so that the flux quantization field and the size of the hysteresis in $I_c(H_x)$ are similar to those in the experimental curves from Fig. 2(a). Figure 5(h) shows the response $I_c(\Phi_y)$ solely to the orthogonal component M_y for different junctions sizes L_x for the sweep from positive to negative field. It is seen that with increasing L_x, the I_c is progressively suppressed in the vicinity of the AP state of the spin valve, where M_y is at maximum.

Figure 5(i) shows the $I_c(H_x)$ modulation, taking into consideration both components of the moment for junctions with fixed L_y and different L_x. According to Ref. [46], it is given by the product of $I_c(\Phi_x)I_c(\Phi_y)$ of curves from Figs. 5(g) and 5(h). It is seen that the first and second side lobes at the negative field, which are close to the AP state, are *suppressed* as a result of the orthogonal M_y component. The effect is *opposite* to our experimental observation in Fig. 2(d), in which side lobes in the vicinity of the AP state are *enhanced*. Therefore, the eventual influence of the M_y component would only strengthen our conclusion and would indicate that the generated amplitude of the spin-triplet component is even larger.

APPENDIX E: ADDITIONAL INDICATIONS OF CONTROLLABLE ENHANCEMENT OF BOTH SPIN-SINGLET AND SPIN-TRIPLET COMPONENTS

In this paper, we presented an analysis of the asymmetry of resistances at half-integer flux quanta, corresponding to maxima of the critical current. Additional information can be obtained from the analysis of junction resistances at zeros of the critical current, corresponding to integer flux quanta, such as points 2, 4, and 6 in Fig. 2(f). It is seen that although points 2 and 4 correspond to the same absolute value of flux through the junction $\Phi/\Phi_0 = \pm 1$, the resistance at point 4 is smaller than that at point 2 [note the reverse scale in Fig. 2(f)]. The difference between those resistances is not due to variation of the critical current (the net Josephson current should be zero at integer flux quanta), but rather it indicates the appearance of an excess quasiparticle conductance in the intermediate layer. Figure 6(a) shows resistances at integer flux quanta for all minima of the critical current seen in Fig. 2(d). The general trend is that the resistance is at maximum in the P state of the spin valve, decreases in the angle state of the spin valve, and reaches minimum in the vicinity of the AP state, marked by a circle. This is *opposite* to the spin-valve magnetoresistance shown in Fig. 1(f). Such behavior has been observed for FSF structures [17,18] and is due to the enhancement of the conventional spin-singlet superconductivity at the intermediate layer due to effective cancellation of opposite exchange fields of the two ferromagnets in the AP state [1,3].

Figures 6(b) and 6(c) show similar data for two SF_1NF_2S junctions with different sizes. Data in panel (c) correspond to $R(H)$ maxima in Fig. 1(e). Here we also show the data for the upward field sweep (black) in order to demonstrate that it is mirror symmetric with respect to the downward sweep (red symbols). In all cases, we observe that the resistance reaches maximum in the P state and exhibits a minimum in the vicinity of the AP state of the spin valve (marked by circles). However, there is an additional minimum on the way from the up-up P state to the AP state. This is where the most noncollinear state of the spin valve should take place, as indicated by red arrows.

In analogy to the $SF_1S'F_2S$ case, we attribute the excess quasiparticle conductance in the AP state of SF_1NF_2S junctions to an enhancement of the proximity-induced spin-singlet order parameter on the intermediate spacer layer of the spin valve. Similarly, the second minimum in resistance is consistent with enhancement of the spin-triplet component of the order parameter at the spacer layer in the noncollinear state of the spin valve [8,10].

In principle, there should be one more noncollinear state upon switching from the antiparallel to the down-down

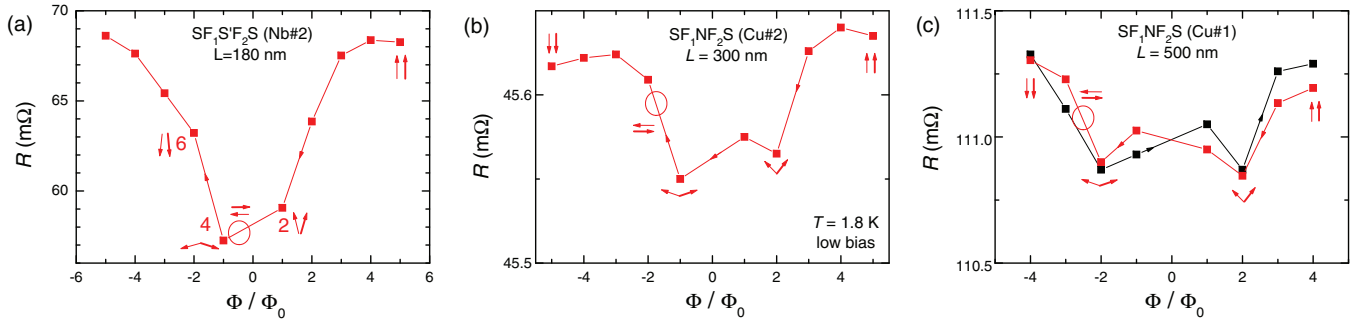

FIG. 6. (Color online) Quasiparticle resistances at integer flux quanta vs the flux through the junction. (a) For the $SF_1S'F_2S$ junction with $L \simeq 180$ nm from Figs. 2(d)–2(f). (b) For the SF_1NF_2S junction with $L \simeq 300$ nm. (c) For the SF_1NF_2S junction with $L \simeq 500$ nm from Fig. 1(e). Red and black symbols represent data for downward and upward field sweeps. Arrows indicate relative orientations of the spin valves. Circles show the position of the AP state. Note the appearance of the minimum of resistance close to the AP state and at the most noncollinear state with $\sim 90^\circ$ angle between magnetization of the ferromagnets. We attribute them to enhancement of the spin-singlet and spin-triplet components of the order parameter, respectively, at the spacer layer.

parallel state. It corresponds to point 5 in Fig. 2(f), at which we observe the enhancement of the supercurrent, attributed to generation of the spin-triplet component of supercurrent through the junction. Therefore, we expect that there should be a third minimum in the quasiparticle resistance between the antiparallel and the down-down parallel states. However, we can measure it only at discrete points, corresponding to integer flux quanta in the junction. In the case of the $SF_1S'F_2S$ junction from Fig. 2(f), the rotation occurs too quickly and at the nearest appropriate point 6 the spin valve is already in the down-down parallel state.

Finally, we note that Fig. 6 indicates that the "normal" resistance of the spin valve is a function of the spin-valve state because of the nontrivial proximity effect in the spacer layer. It is important to emphasize that such behavior does not affect out conclusions. On the contrary, from Figs. 2(f) and 6(a) it is seen that while the peak at the noncollinear point 5 is higher than at the corresponding almost collinear point 1, the adjacent minimum at point 4 is deeper than at point 2. This makes the relative height difference between the noncollinear peak 5-4 and the corresponding almost collinear peak 1-2 even larger.

[1] A. I. Buzdin, Rev. Mod. Phys. **77**, 935 (2005).
[2] F. S. Bergeret, A. F. Volkov, and K. B. Efetov, Rev. Mod. Phys. **77**, 1321 (2005).
[3] Ya. V. Fominov, A. A. Golubov, and M. Yu. Kupriyanov, JETP Lett. **77**, 510 (2003).
[4] Ya. M. Blanter and F. W. J. Hekking, Phys. Rev. B **69**, 024525 (2004).
[5] J. Kopu, M. Eschrig, J. C. Cuevas, and M. Fogelström, Phys. Rev. B **69**, 094501 (2004).
[6] M. Houzet and A. I. Buzdin, Phys. Rev. B **76**, 060504 (2007).
[7] Y. Asano, Y. Sawa, Y. Tanaka, and A. A. Golubov, Phys. Rev. B **76**, 224525 (2007).
[8] L. Trifunovic, Z. Popovic, and Z. Radovic, Phys. Rev. B **84**, 064511 (2011).
[9] A. S. Mel'nikov, A. V. Samokhvalov, S. M. Kuznetsova, and A. I. Buzdin, Phys. Rev. Lett. **109**, 237006 (2012).
[10] N. G. Pugach and A. I. Buzdin, Appl. Rev. Lett. **101**, 242602 (2012).
[11] M. Alidoust, G. Sewell, and J. Linder, Phys. Rev. Lett. **108**, 037001 (2012).
[12] V. T. Petrashov, I. A. Sosnin, I. Cox, A. Parsons, and C. Troadec, Phys. Rev. Lett. **83**, 3281 (1999).
[13] J. Wang, M. Singh, M. Tian, N. Kumar, B. Liu, C. Shi, J. K. Jain, N. Samarth, T. E. Mallouk, and M. H. W. Chan, Nat. Phys. **6**, 389 (2010).
[14] V. Pena, Z. Sefrioui, D. Arias, C. Leon, J. Santamaria, M. Varela, S. J. Pennycook, and J. L. Martinez, Phys. Rev. B **69**, 224502 (2004).
[15] R. S. Keizer, S. T. B. Goennenwein, T. M. Klapwijk, G. Miao, G. Xiao, and A. Gupta, Nature (London) **439**, 825 (2006).
[16] T. Golod, A. Rydh, V. M. Krasnov, I. Marozau, M. A. Uribe-Laverde, D. K. Satapathy, Th. Wagner, and C. Bernhard, Phys. Rev. B **87**, 134520 (2013).
[17] B. Li, N. Roschewsky, B. A. Assaf, M. Eich, M. Epstein-Martin, D. Heiman, M. Münzenberg, and J. S. Moodera, Phys. Rev. Lett. **110**, 097001 (2013).
[18] N. Banerjee, C. B. Smiet, R. G. J. Smits, A. Ozaeta, F. S. Bergeret, M. G. Blamire, and J. W. A. Robinson, Nat. Commun. **5**, 3048 (2014).
[19] P. V. Leksin, N. N. Garif'yanov, I. A. Garifullin, J. Schumann, V. Kataev, O. G. Schmidt, and B. Büchner, Phys. Rev. Lett. **106**, 067005 (2011).
[20] C. Bell, G. Burnell, C. W. Leung, E. J. Tarte, D.-J. Kang, and M. G. Blamire, Appl. Phys. Lett. **84**, 1153 (2004).
[21] T. S. Khaire, M. A. Khasawneh, W. P. Pratt, Jr., and N. O. Birge, Phys. Rev. Lett. **104**, 137002 (2010).
[22] J. W. A. Robinson, G. B. Halasz, A. I. Buzdin, and M. G. Blamire, Phys. Rev. Lett. **104**, 207001 (2010).
[23] B. Baek, W. H. Rippard, S. P. Benz, S. E. Russek, and P. D. Dresselhaus, Nat. Commun. **5**, 3888 (2014).
[24] T. Golod, A. Rydh, and V. M. Krasnov, Phys. Rev. Lett. **104**, 227003 (2010).
[25] I. S. Veshchunov, V. A. Oboznov, A. N. Rossolenko, A. S. Prokofiev, L. Ya. Vinnikov, A. Yu. Rusanov, and D. V. Matveev, JETP Lett. **88**, 758 (2008).
[26] B. Dieny, V. S. Speriosu, S. S. P. Parkin, B. A. Gurney, D. R. Wilhoit, and D. Mauri, Phys. Rev. B **43**, 1297 (1991).
[27] V. V. Bol'ginov, V. S. Stolyarov, D. S. Sobanin, A. L. Karpovich, and V. V. Ryazanov, JETP Lett. **95**, 366 (2012).
[28] V. M. Krasnov, V. A. Oboznov, and N. F. Pedersen, Phys. Rev. B **55**, 14486 (1997).
[29] N. Banerjee *et al.*, Nat. Commun. **5**, 4771 (2014).
[30] C. L. Dennis, R. P. Borges, L. D. Buda, U. Ebels, J. F. Gregg, M. Hehn, E. Jouguelet, K. Ounadjela, I. Petej, I. L. Prejbeanu, and M. J. Thornton, J. Phys.: Condens. Matter **14**, R1175 (2002).
[31] B. Kaplan and G. A. Gehring, J. Magn. Magn. Mater. **128**, 111 (1993).
[32] A. Stankiewicz, S. J. Robinson, G. A. Gehring, and V. V. Tarasenko, J. Phys.: Condens. Matter **9**, 1019 (1997).
[33] Yu. I. Bespyatykh, E. H. Lock, S. A. Nikitov, and W. Wasilewski, J. Magn. Magn. Mater. **195**, 555 (1999).
[34] I. S. Veshchunov, Ph.D. thesis, Institute of Solid State Physics, Russian Academy of Science, Chernogolovka, 2010.
[35] R. L. Coren, J. Appl. Phys. **37**, 230 (1966).
[36] H. Chang and J. Burns, J. Appl. Phys. **37**, 3240 (1966).
[37] M. Wu and W. Abdul-Razzaq, Phys. Rev. B **42**, 4590 (1990).
[38] T. Golod, A. Rydh, and V. M. Krasnov, J. Appl. Phys. **110**, 033909 (2011); T. Golod, A. Rydh, P. Svedlindh, and V. M. Krasnov, Phys. Rev. B **87**, 104407 (2013).
[39] M. Flokstra and J. Aarts, Phys. Rev. B **80**, 144513 (2009).
[40] Z. B. Guo, W. B. Mi, Q. Zhang, B. Zhang, R. O. Aboljadayel, and X. X. Zhang, Solid State Commun. **152**, 220 (2012).
[41] A. Iovan *et al.* (unpublished).
[42] T. S. Khaire, W. P. Pratt, Jr., and N. O. Birge, Phys. Rev. B **79**, 094523 (2009).
[43] A. Yu. Aladyshkin, A. V. Silhanek, W. Gillijns, and V. V. Moshchalkov, Supercond. Sci. Technol. **22**, 053001 (2009).
[44] Simulations were performed using OOMMF software, http://math.nist.gov/oommf/.
[45] M. Weides, Appl. Phys. Lett. **93**, 052502 (2008).
[46] A. Barone and C. Paterno, *Physics and Applications of the Josephson Effect* (Wiley, New York, 1982).